Scalable Creation of Long-Lived Multipartite Entanglement

H. Kaufmann, T. Ruster, C. T. Schmiegelow, M. A. Luda, V. Kaushal, J. Schulz, D. von Lindenfels, F. Schmidt-Kaler, and U. G. Poschinger

Phys. Rev. Lett. **119**, 150503 — Published 13 October 2017

DOI: 10.1103/PhysRevLett.119.150503

Scalable creation of long-lived multipartite entanglement

H. Kaufmann,[1] T. Ruster,[1] C. T. Schmiegelow,[1,*] M. A. Luda,[1,†] V. Kaushal,[1]
J. Schulz,[1] D. von Lindenfels,[1] F. Schmidt-Kaler,[1] and U. G. Poschinger[1,‡]

[1] *Institut für Physik, Universität Mainz, Staudingerweg 7, 55128 Mainz, Germany*

We demonstrate the deterministic generation of multipartite entanglement based on scalable methods. Four qubits are encoded in $^{40}Ca^{+}$, stored in a micro-structured segmented Paul trap. These qubits are sequentially entangled by laser-driven pairwise gate operations. Between these, the qubit register is dynamically reconfigured via ion shuttling operations, where ion crystals are separated and merged, and ions are moved in and out of a fixed laser interaction zone. A sequence consisting of three pairwise entangling gates yields a four-ion GHZ state $|\psi\rangle = \frac{1}{\sqrt{2}}(|0000\rangle + |1111\rangle)$, and full quantum state tomography reveals a state fidelity of 94.4(3)%. We analyze the decoherence of this state and employ dynamic decoupling on the spatially distributed constituents to maintain 69(5)% coherence at a storage time of 1.1 seconds.

The key challenge for the realization of quantum information processing devices which actually outperform classical information technology lies in the scaling to a sufficient complexity, while maintaining high operational fidelities. With trapped ions and superconducting circuits being the leading candidates for scalable high-fidelity quantum computing (QC) platforms, few-qubit architectures have been realized [1, 2], and elementary quantum algorithms [3, 4] as well as building blocks for quantum error correction [5, 6] have been demonstrated. For trapped ions, a route to scalability was opened up with the seminal proposal of the *quantum CCD* [7], where ions are stored in segmented, micro-chip-based radiofrequency traps [8, 9] and shuttled between distinct trap sites in order to realize quantum logic operations on selected subgroups of qubits [10–14]. Based on these methods, a complete methods set for QC [15] and a fully programmable two-qubit quantum processor [16] have been shown. It is rather likely that any trapped-ion based large-scale QC architecture [17–19] will involve ion shuttling operations.

As a benchmark for QC capabilities, the generation and properties of multipartite entangled states have been studied intensively. On the one hand, generating and maintaining such states lies at the heart of QC, on the other hand large multipartite entangled states represent a resource for the measurement-based QC approach [20, 21]. The first generation of a four-particle Greenberger-Horne-Zeilinger (GHZ) states has been accomplished at a state fidelity of 57% by the NIST group [22], while eight-qubit W-states at 76% fidelity have been created later by the Innsbruck group [23]. Furthermore, GHZ states of up to 14 trapped ions have been created [24], and it has been shown that these states are rather fragile in the presence of correlated noise. While large-scale entanglement of thousands of optical modes [25] or atoms [26] has also been demonstrated, QC requires *deterministic* entanglement generation with capabilities for storage and *individual* manipulation and readout of the qubits.

In this work, we demonstrate the scalable generation of GHZ states of up to four trapped ions. This work constitutes the first demonstration of multipartite entanglement generation featuring full local high-fidelity control over the constituents in terms of qubit state *and* position. This marks an important milestone towards the realization of quantum computing with trapped ions in a scalable architecture. Our method is based on single-qubit rotations, pairwise two-qubit entangling gates and shuttling operations. Gate operations are driven by laser beams which are directed to one fixed trap site, the laser interaction zone (LIZ). By shuttling only the required ions to this trap site, crosstalk is strongly suppressed as compared to static ion-crystal registers, as memory ions, which are not to be affected by gate operations, are stored several hundreds of microns away from the LIZ. Furthermore, it has been shown that the coherence of GHZ states is fragile in the presence of correlated local magnetic field noise [24]. Here, we demonstrate that the GHZ coherence can be maintained by dynamical decoupling (DD) on the distributed components, leading to an increase of the coherence time of a four-qubit GHZ state by roughly two orders of magnitude.

The centerpiece of our quantum processor is the segmented Paul trap shown in Fig. 1, which is similar to the trap described in Ref. [27]. Quantum information is encoded in the Zeeman sublevels of the ground state of trapped $^{40}Ca^{+}$ ions $|0\rangle \equiv |\downarrow\rangle \equiv |S_{1/2}, m_J = -\frac{1}{2}\rangle$ and $|1\rangle \equiv |\uparrow\rangle \equiv |S_{1/2}, m_J = +\frac{1}{2}\rangle$. The Zeeman sublevels are separated by $2\pi\times 10.5\,\mathrm{MHz}$ by a magnetic field, which is generated by permanent magnets. The trap is placed in a μ-metal enclosure for shielding of fluctuating ambient magnetic fields, and all experiments are synchronized to the ac line frequency. This yields a Ramsey coherence time of around 300 ms [28] for a single qubit.

Laser light is employed for Doppler cooling (397 nm), qubit state initialization and qubit readout (729 nm), see Ref. [29]. For a fluorescence detection time of 1.2 ms, we

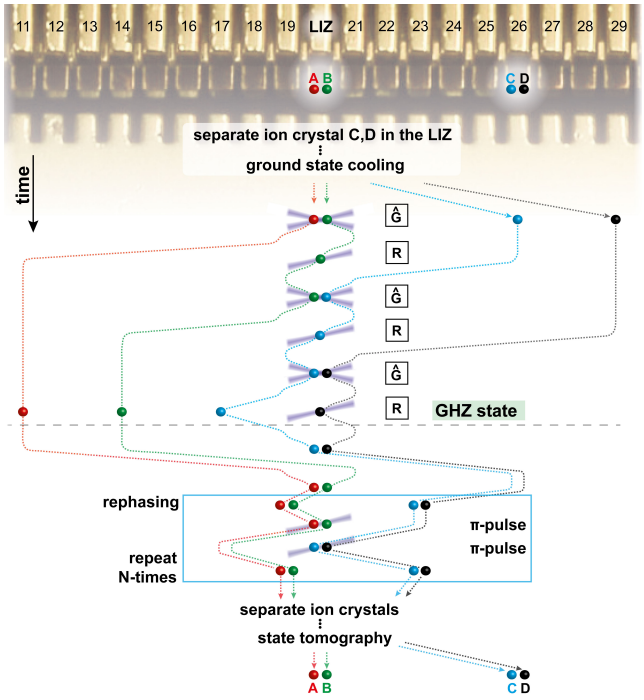

FIG. 1. Shuttling sequence for the creation, storage and analysis of a four-ion GHZ state. State creation takes place above the dashed line. Entangling gates $\hat{G}$ and single qubit rotations $\hat{R}$ are carried out in the laser interaction zone (LIZ). After the GHZ state is created, it can be stored for hundreds of ms by employing DD. The ions are not stored in the LIZ to prevent depolarization from residual light near the cycling transition.

achieve a spin measurement fidelity of 99.92% for a single ion. A separate laser source near 397 nm is used to manipulate the qubits via stimulated Raman transitions at a detuning of about $-2\pi\times290$ GHz from the $S_{1/2} \leftrightarrow P_{1/2}$ transition. Entangling gates at sufficiently good fidelity require cooling the ions close to the motional ground state [30], for which a pair of orthogonally propagating beams is employed. As the difference wave vector is oriented orthogonally to the trap axis, the lasers couple to the radial secular modes. A second pair of identically aligned beams is used for pairwise qubit entanglement via a geometric phase gate [31].

Shuttling operations take place along the trap (x)-axis, and can therefore cause motional excitation along this direction. The cost for mitigating these excitations are excessive calibration overhead and increase of operational time via slower shuttling. Especially for separation, axial excitation can be only partially mitigated, at the requirement of carefully calibrated parameters [13, 32]. Therefore, all sensitive operations are carried out such that they are robust with respect to excitation of the axial ion motion: the entangling gate (driven on a radial secular mode), single qubit rotations (driven by co-propagating laser beams) and spin readout via electron shelving to the metastable $D_{5/2}$ state by 729 nm light (laser beam directed perpendicular to trap axis). Typical secular trap frequencies are: $\omega_{x,y,z}= 2\pi \times \{1.5, 4.1, 4.9\}$ MHz, where x denotes the trap axis. Ions are shuttled along this direction by applying time-dependent waveforms to the dc electrodes of the linear Paul trap [12, 13]. To ensure a high entangling gate fidelity on a radial secular mode, the amplitude of the $2\pi\times33$ MHz rf trap drive is actively stabilized. We find the long-term relative stability of the radial secular frequencies to be about 5 ppm. Heating rates on the different secular modes, measured at the LIZ, range between 3(1) quanta per second for the radial z mode and 20(1) for the axial x mode.

The experimental toolbox comprises a set of techniques, which we describe in the following. Since the entangling gates require the ions to be close to the ground state of the radial motion, we apply resolved sideband cooling to all ions. A single cooling pulse takes on average 15 µs. We either cool single ions or pairs of two ions and cool all radial modes with 40 pulses per mode.

A single qubit π-rotation is realized by a 10 µs pulse. Using randomized benchmarking [33], we determine an error per gate as low as $5.1(2)\times10^{-5}$. We also perform qubit rotations on two ions simultaneously, for which we calibrate the relative imbalance in terms of Rabi frequency to better than 1.5×10^{-5}.

The entangling gate is driven by spin-dependent optical dipole forces [31], generating the unitary $\hat{G} = \mathrm{diag}(1, i, i, 1)$. At a detuning of $2\pi\times$ 25 kHz from the higher-frequency radial center-of-mass mode, the gate operation takes 100 µs. We achieve a Bell-state fidelity of 99.0(4)%. The gate is used, in conjunction with local rotations, to generate the "entanglement seeding" unitary $\hat{U}_1$ and the "sequential CNOT" unitary $\hat{U}_2$:

$$\hat{U}_1 = \frac{e^{i\pi/4}}{\sqrt{2}}\begin{pmatrix} 1 & 0 & 0 & i \\ 0 & 1 & -i & 0 \\ 0 & -i & 1 & 0 \\ i & 0 & 0 & 1 \end{pmatrix}, \quad \hat{U}_2 = \begin{pmatrix} 0 & 1 & 0 & 0 \\ -i & 0 & 0 & 0 \\ 0 & 0 & i & 0 \\ 0 & 0 & 0 & 1 \end{pmatrix}. \tag{1}$$

The sequential CNOT $\hat{U}_2$ requires shuttling of a single ion to the LIZ for a local rotation, a subsequent recombination of two ions in the LIZ for an entangling gate, followed by a separation operation and a final transport of a single ion to the LIZ for a single local rotation. The infidelities of both single qubit rotations and two-qubit gates are predominantly given by off-resonant photon scattering, as determined from comparison with expected scattering-induced errors at the given operating parameters, i.e. Raman detuning and gate durations [34].

Ion shuttling along the trap axis is performed by concatenated segment-to-segment transports of 200 µm, where each operation takes 30 µs. We estimate the motional excitation on the radial modes to be below 0.01 phonons per transport. Separation of a two-ion crystal is realized by increasing the voltage on the trapping segment and lowering the voltage on the adjacent segments

[13, 32] within 160 µs. The operation and its reverse-counterpart – the recombination of two individual ions – are carried out in the LIZ as it requires careful calibration of the electrode voltages via measurements of motional frequencies. Separation and recombination lead to an excitation of about 0.05 phonons on the gate mode.

We employ a sequence of two-ion entangling gates and single qubit operations to create an entangled GHZ state $|\Psi\rangle = 1/\sqrt{2}\,(i\,|0000\rangle + |1111\rangle)$. The sequence, including shuttling operations, is sketched in Fig. 1. It is comprised of five blocks: An initial *cooling block* prepares the ions close to the ground state of motion of the radial secular modes, which is crucial for high-fidelity gate operations in the subsequent quantum logic block. After state preparation, the coherence can be maintained through an optional *rephasing block*. To analyze the final state, quantum state tomography is performed in the *analysis block*. A *final block* contains a magnetic field tracking measurement and an ion repositioning sequence which enables the next repetition of the entire sequence. In the following, we describe these operational blocks.
Initially, ion pair A, B is stored at electrode 20 in the LIZ and ion pair C, D is stored at electrode 26. Ion pair A, B is then shuttled to electrode 14 and pair C, D is shuttled to the LIZ for a separation operation which transfers ion C to electrode 19 and ion D to electrode 21. Ion pair A, B and the single ions C and D are consecutively transported to the LIZ for resolved sideband cooling and spin initialization to $|\psi\rangle = |1111\rangle$. Subsequently, we perform quantum logic operations to generate the maximally entangled GHZ state via the quantum circuit shown in Fig. 2, which is comprised of one- and two-qubit quantum logic operations. Application of the unitary $\hat{U}_1$ on the ion pair A, B in the LIZ generates the state $|\psi\rangle = (i\,|0011\rangle + |1111\rangle)/\sqrt{2}$, where ions A and B are entangled. The entanglement is extended to all qubits by subsequent application of the C-NOT unitary $\hat{U}_2$ on qubits B,C and C,D. This leads to the final state $|\psi\rangle = (i\,|0000\rangle + |1111\rangle)/\sqrt{2}$, with the constituent qubits distributed over a macroscopic distance of 1.8 mm.

Since qubits in superposition states are shuttled along the trap axis, they accumulate a phase ϕ due to the inhomogeneous magnetic field [35]. In total, four of these phases need to be considered in the quantum gate sequence. We find each of them to be constant over time and to be $\phi < \pm 0.6$ rad. The phase is compensated for by adjusting the phase of an adjacent single qubit rotation, see Fig. 2 c).

We perform quantum state tomography by subsequent shuttling of each of the ions to the LIZ. For each ion, one of the analysis rotations $\{\mathbb{1}, R_X(\pi/2), R_Y(\pi/2)\}$ is carried out in order to measure the operators $\{\sigma_z, \sigma_y, \sigma_x\}$. As we are only interested in the GHZ state fidelity irrespective of the relative phase (see below), the analysis pulses are not corrected for additional phase accumulation occurring during shuttling operations after the last

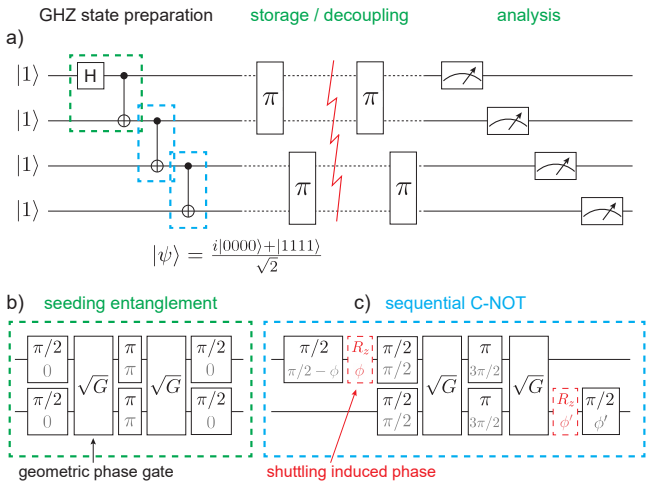

FIG. 2. (a) Quantum circuit for the creation, storage and analysis of a four-ion GHZ state. The state is generated by three subsequent entangling gates. Evenly spaced DD π-pulses are employed to achieve long coherence times, followed by state tomography on the individual ions. The green (b) and blue (c) dashed boxes show how the respective entangling gates are realized in the experiment – they correspond to the unitary operators $\hat{U}_1$ and $\hat{U}_2$, from Eq. 1. The upper numbers in the boxes indicating the single qubit operations represent the laser pulse areas, whereas the lower numbers indicate the phase of the respective pulse. Red boxes represent an additional phase which arises from the shuttling operations, see text.

entangling gate.

After the application of tomography rotations, each ion is shuttled to the LIZ for population transfer $|\uparrow\rangle \leftrightarrow |D_{5/2}\rangle$ via electron shelving. The ions are again individually shuttled to the LIZ, where state-dependent fluorescence is observed. All qubits are shelved *before* fluorescence detection, to avoid depolarization of a remotely stored qubit from scattered light near 397 nm.

After measurement, we carry out the magnetic field tracking block. Ion A, placed at the LIZ, is used to measure the drift of the qubit frequency in two Ramsey experiments with 5 ms interrogation time, and 0° and 90° analysis phase, respectively. From these two measurements, we infer the deviation from the actual qubit frequency, and correct it for subsequent measurement cycles. Finally, the ions are merged into pairs and the entire sequence is repeated. In order to obtain the fidelity of the prepared state, we reconstruct density matrices $\hat{\rho}$ from the measurement data and compute the state fidelity

$$\mathcal{F}(\hat{\rho}) = \max_{\theta} \langle\Psi(\theta)|\,\hat{\rho}\,|\Psi(\theta)\rangle \qquad (2)$$

with respect to a GHZ state of arbitrary relative phase θ:

$$|\Psi(\theta)\rangle = \tfrac{1}{\sqrt{2}}\left(|0000\rangle + e^{i\theta}\,|1111\rangle\right). \qquad (3)$$

We first perform linear inversion of the measurement data, which consists of 4×50900 measurements in total.

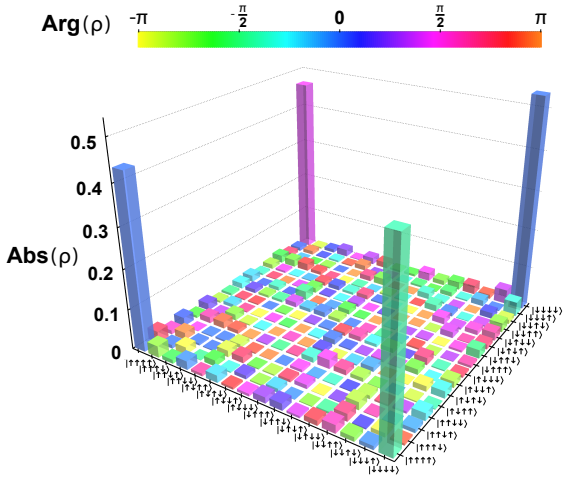

FIG. 3. Reconstructed density matrix of a maximally entangled four-ion GHZ state with correction for readout errors. Linear reconstruction with correction for SPAM errors yields a state fidelity of $\mathcal{F} = 94.38\%$. We determine the GHZ phase (see Eq. 3) to $\theta = -2\pi \times 0.217(2)$.

This yields a density matrix, from which a fidelity of $\mathcal{F}$ =92.60% is extracted. As a density matrix obtained from linear inversion can feature negative eigenvalues due to statistical errors, the density matrix obtained from linear inversion is not suitable for estimation of a confidence interval via parametric bootstrapping. We additionally perform a maximum-likelihood (ML) state reconstruction [36]. Using the physical density matrix from the ML reconstruction for parametric bootstrapping, we estimate a fidelity of $\mathcal{F}_{ML}$ =92.50(37)%, such that linear inversion and ML estimation yield consistent results.

By running the sequence without quantum logic operations, we determine the readout errors [29]. State preparation and measurement (SPAM) errors are dominated by the limited lifetime of the $D_{5/2}$ state of 1.2 s. E. g., for ion A, the time between shelving and fluorescence detection is 2.7 ms, leading to an estimated decay-induced SPAM error of 0.2%. An actual error of 0.4% is measured for ion A, the remaining error is attributed to shuttling-induced motional excitation, which affects the shelving efficiency. This is either due to residual coupling of 729 nm shelving laser to axial motion, or due to residual radial excitation from shuttling. Including correction for SPAM errors, the fidelity obtained from linear inversion is $\mathcal{F}$ =94.38%. The obtained density matrix is displayed in Fig. 3. Here, ML estimation with parametric bootstrapping yields $\mathcal{F}_{ML}$ =94.28(30)%. Additionally, we perform statistical tests based on Hoeffding's tail inequality [37], confirming that the measurement data is statistically consistent with the state described by the reconstructed density matrices.

The theoretical fidelity limit for our setting is 97%, since the two-qubit entangling gate is performed three times at a fidelity of 99.0(4)%. We attribute the discrepancy from this result to imperfect calibration of the individually calibrated entangling gates and the correction phases ϕ, as well as the finite accuracy of the magnetic field tracking measurements. The entangling gates require individual calibration due to small motional excitation – mainly from heating – which results in a reduced coupling to the driving field and thus requires a slightly increased power the entangling gate pulse.

The execution time for the creation of the GHZ state after sideband cooling is 3.1 ms, where 11% is used for quantum gates and the remainder is dedicated to shuttling operations. This illustrates that currently, the shuttling overhead dominates the time budget of the quantum CCD operation. However, a significant leeway for optimization of these operations via technological and methodological improvements exists.

Magnetically sensitive multi-qubit GHZ states are prone to *super-decoherence*, which is caused by correlated local magnetic field noise [24]. We measure the coherence time of a four-ion GHZ state and employ DD to achieve extended lifetimes. Here, repeated π-flips of the qubits serve to effectively cancel the coupling of the qubits to a drifting offset magnetic field [38]. Once the GHZ state is created, the four individually trapped ions are merged to ion pairs A, B and C, D to reduce the amount of shuttling operations in the rephasing block. After storing the ion pairs at segments 19 and 23, they are alternately shuttled to the LIZ and subjected to π-pulses. The pulses are evenly spaced within the storage time, thus only an odd number of pulses is suitable for decoupling. After the rephasing block, the ion pairs are separated into individually trapped ions for state analysis. We utilize a reduced measurement scheme, by measuring the operators $\{\sigma_x^{(A)}\sigma_x^{(B)}\sigma_x^{(C)}\sigma_x^{(D)}\}$ and $\{\sigma_x^{(A)}\sigma_x^{(B)}\sigma_x^{(C)}\sigma_y^{(D)}\}$. To infer the GHZ coherence of the state, each of the two operators is measured at least 200 times. The GHZ coherence and its statistical measurement error are determined from the measurement results via ML parameter estimation [35]. The results of these measurements are shown in Fig. 4. The coherence time of the GHZ state without rephasing pulses is about 20 ms. By applying $N_\pi = 15$ rephasing pulses on each ion pair, we achieve coherence times exceeding one second. As can be seen from Fig. 4, the coherence does not decrease monotonically. We attribute this to noise at frequencies that match the inverse time difference between subsequent decoupling pulses [39].

In conclusion, we demonstrate the creation of an entangled four-qubit GHZ state in a trapped-ion quantum processor using a scalable technique, attaining a state fidelity comparable to previous realizations in non-scalable, static settings [24]. We employ DD to preserve the coherence of the sensitive entangled state for more than one second. We achieve the *deterministic* generation of multipartite entangled state, with its constituents distributed over a *macroscopic range*, which persists for unprecedented *long storage times*.

The combination of shuttling-insensitive gates long co-

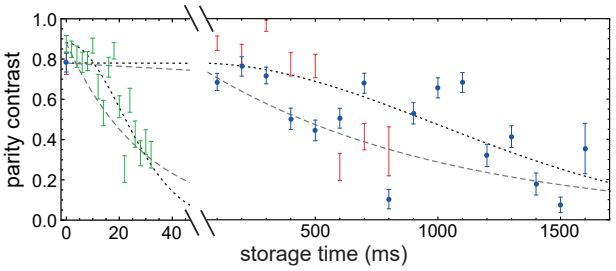

FIG. 4. Preservation of the parity contrast of a four-ion GHZ state by DD. Green triangles for short times correspond to a measurement without the execution of the rephasing block. Blue circles represent a measurement with $N_\pi = 15$ rephasing pulses on each qubit, while red squares correspond to $N_\pi = 3$. The dotted black line represents a Gaussian decay, whereas the grey dashed line represents an exponential decay. The data shown is not corrected for SPAM errors.

herence times will enable our quantum processor to execute quantum algorithms of increasing complexity. Faster shuttling operations will increase the operational speed. In conjunction with physical two-ion SWAP gates - which have been realized in our trap [29] - and feed-forward quantum logic, our setup will be extended to a freely programmable QC platform.

The research is based upon work supported by the Office of the Director of National Intelligence (ODNI), Intelligence Advanced Research Projects Activity (IARPA), via the U.S. Army Research Office grant W911NF-16-1-0070. The views and conclusions contained herein are those of the authors and should not be interpreted as necessarily representing the official policies or endorsements, either expressed or implied, of the ODNI, IARPA, or the U.S. Government. The U.S. Government is authorized to reproduce and distribute reprints for Governmental purposes notwithstanding any copyright annotation thereon. Any opinions, findings, and conclusions or recommendations expressed in this material are those of the author(s) and do not necessarily reflect the view of the U.S. Army Research Office. We acknowledge helpful discussions with Philipp Schindler and Alex Retzker, and financial support from the DFG through the DIP program (Grant No. SCHM 1049/7-1).

* Present address: LIAF - Laboratorio de Iones y Atomos Frios, Departamento de Fisica & Instituto de Fisica de Buenos Aires, 1428 Buenos Aires, Argentina
† Present address: DEILAP, CITEDEF & CONICET, J.B. de La Salle 4397, 1603 Villa Martelli, Buenos Aires, Argentina
‡ poschin@uni-mainz.de

[1] J. Kelly, R. Barends, A. G. Fowler, A. Megrant, E. Jeffrey, T. C. White, D. Sank, J. Y. Mutus, B. Campbell, Y. Chen, Z. Chen, B. Chiaro, A. Dunsworth, I.-C. Hoi, C. Neill, P. J. J. O'Malley, C. Quintana, P. Roushan, A. Vainsencher, J. Wenner, A. N. Cleland, and J. M. Martinis, Nature **519**, 66 (2015).
[2] P. Schindler, D. Nigg, T. Monz, J. T. Barreiro, E. Martinez, S. X. Wang, S. Quint, M. F. Brandl, V. Nebendahl, C. F. Roos, M. Chwalla, M. Hennrich, and R. Blatt, New Journal of Physics **15**, 123012 (2013).
[3] T. Monz, D. Nigg, E. A. Martinez, M. F. Brandl, P. Schindler, R. Rines, S. X. Wang, I. L. Chuang, and R. Blatt, Science **351**, 1068 (2016).
[4] S. Debnath, N. M. Linke, C. Figgatt, K. A. Landsman, K. Wright, and C. Monroe, Nature **536**, 63 (2016).
[5] J. M. Chow, J. M. Gambetta, E. Magesan, D. W. Abraham, A. W. Cross, B. R. Johnson, N. A. Masluk, C. A. Ryan, J. A. Smolin, S. J. Srinivasan, and M. Steffen, Nature Communications **5**, 4015 EP (2014), article.
[6] D. Nigg, M. Müller, E. A. Martinez, P. Schindler, M. Hennrich, T. Monz, M. A. Martin-Delgado, and R. Blatt, Science **345**, 302 (2014).
[7] D. Kielpinski, C. Monroe, and D. J. Wineland, Nature **417**, 709 (2002).
[8] S. Seidelin, J. Chiaverini, R. Reichle, J. J. Bollinger, D. Leibfried, J. Britton, J. H. Wesenberg, R. B. Blakestad, R. J. Epstein, D. B. Hume, W. M. Itano, J. D. Jost, C. Langer, R. Ozeri, N. Shiga, and D. J. Wineland, Phys. Rev. Lett. **96**, 253003 (2006).
[9] W. K. Hensinger, S. Olmschenk, D. Stick, D. Hucul, M. Yeo, M. Acton, L. Deslauriers, C. Monroe, and J. Rabchuk, Applied Physics Letters **88**, 034101 (2006).
[10] M. A. Rowe, A. Ben-Kish, B. DeMarco, D. Leibfried, V. Meyer, J. Beall, J. Britton, J. Hughes, W. M. Itano, B. Jelenkovic, C. Langer, T. Rosenband, and D. J. Wineland, Quantum Inf. and Comput. **2**, 257 (2002).
[11] R. Bowler, J. Gaebler, Y. Lin, T. R. Tan, D. Hanneke, J. D. Jost, J. P. Home, D. Leibfried, and D. J. Wineland, Phys. Rev. Lett. **109**, 080502 (2012).
[12] A. Walther, F. Ziesel, T. Ruster, S. T. Dawkins, K. Ott, M. Hettrich, K. Singer, F. Schmidt-Kaler, and U. G. Poschinger, Phys. Rev. Lett. **109**, 080501 (2012).
[13] T. Ruster, C. Warschburger, H. Kaufmann, C. T. Schmiegelow, A. Walther, M. Hettrich, A. Pfister, V. Kaushal, F. Schmidt-Kaler, and U. G. Poschinger, Phys. Rev. A **90**, 033410 (2014).
[14] S. D. Fallek, C. D. Herold, B. J. McMahon, K. M. Maller, K. R. Brown, and J. M. Amini, New Journal of Physics **18**, 083030 (2016).
[15] J. P. Home, D. Hanneke, J. D. Jost, J. M. Amini, D. Leibfried, and D. J. Wineland, Science **325**, 1227 (2009).
[16] D. Hanneke, J. P. Home, J. D. Jost, J. M. Amini, D. Leibfried, and D. J. Wineland, Nat Phys **6**, 13 (2010).
[17] B. Lekitsch, S. Weidt, A. G. Fowler, K. Mølmer, S. J. Devitt, C. Wunderlich, and W. K. Hensinger, Science Advances **3** (2017), 10.1126/sciadv.1601540.
[18] C. Monroe, R. Raussendorf, A. Ruthven, K. R. Brown, P. Maunz, L.-M. Duan, and J. Kim, Phys. Rev. A **89**, 022317 (2014).
[19] M. F. Brandl, (2017), arXiv:1702.02583.
[20] R. Raussendorf and H. J. Briegel, Phys. Rev. Lett. **86**, 5188 (2001).
[21] B. P. Lanyon, P. Jurcevic, M. Zwerger, C. Hempel, E. A. Martinez, W. Dür, H. J. Briegel, R. Blatt, and C. F. Roos, Phys. Rev. Lett. **111**, 210501 (2013).
[22] C. A. Sackett, D. Kielpinski, B. E. King, C. Langer, V. Meyer, C. J. Myatt, M. Rowe, Q. A. Turchette, W. M. Itano, D. J. Wineland, and C. Monroe, Nature **404**, 256

(2000).
[23] H. Häffner, W. Hänsel, C. F. Roos, J. Benhelm, D. Chekal kar, M. Chwalla, T. Körber, U. D. Rapol, M. Riebe, P. O. Schmidt, C. Becher, O. Gühne, W. Dür, and R. Blatt, Nature **438**, 643 (2005).
[24] T. Monz, P. Schindler, J. T. Barreiro, M. Chwalla, D. Nigg, W. A. Coish, M. Harlander, W. Hänsel, M. Hennrich, and R. Blatt, Phys. Rev. Lett. **106**, 130506 (2011).
[25] S. Yokoyama, R. Ukai, S. C. Armstrong, C. Sornphiphatphong, T. Kaji, S. Suzuki, J.-i. Yoshikawa, H. Yonezawa, N. C. Menicucci, and A. Furusawa, Nat Photon **7**, 982 (2013).
[26] R. McConnell, H. Zhang, J. Hu, S. Cuk, and V. Vuletic, Nature **519**, 439 (2015).
[27] S. A. Schulz, U. Poschinger, F. Ziesel, and F. Schmidt-Kaler, New Journal of Physics **10**, 045007 (2008).
[28] T. Ruster, C. T. Schmiegelow, H. Kaufmann, C. Warschburger, F. Schmidt-Kaler, and U. G. Poschinger, Applied Physics B **122**, 254 (2016).
[29] H. Kaufmann, T. Ruster, C. T. Schmiegelow, M. A. Luda, V. Kaushal, J. Schulz, D. von Lindenfels, F. Schmidt-Kaler, and U. G. Poschinger, Phys. Rev. A **95**, 052319 (2017).
[30] C. J. Ballance, *High-Fidelity Quantum Logic in* Ca^+, dissertation, University of Oxford (2014).
[31] D. Leibfried, B. DeMarco, V. Meyer, D. Lucas, M. Barrett, J. Britton, W. M. Itano, B. Jelenkovic, C. Langer, T. Rosenband, and D. J. Wineland, Nature **422**, 412 (2003).
[32] H. Kaufmann, T. Ruster, C. T. Schmiegelow, F. Schmidt-Kaler, and U. G. Poschinger, New Journal of Physics **16**, 073012 (2014).
[33] E. Knill, D. Leibfried, R. Reichle, J. Britton, R. B. Blakestad, J. D. Jost, C. Langer, R. Ozeri, S. Seidelin, and D. J. Wineland, Phys. Rev. A **77**, 012307 (2008).
[34] R. Ozeri, W. M. Itano, R. B. Blakestad, J. Britton, J. Chiaverini, J. D. Jost, C. Langer, D. Leibfried, R. Reichle, S. Seidelin, J. H. Wesenberg, and D. J. Wineland, Phys. Rev. A **75**, 042329 (2007).
[35] T. Ruster, H. Kaufmann, M. A. Luda, V. Kaushal, C. T. Schmiegelow, F. Schmidt-Kaler, and U. G. Poschinger, (2017), arXiv:1704.01793.
[36] J. Řeháček, Z. Hradil, E. Knill, and A. I. Lvovsky, Phys. Rev. A **75**, 042108 (2007).
[37] T. Moroder, M. Kleinmann, P. Schindler, T. Monz, O. Gühne, and R. Blatt, Phys. Rev. Lett. **110**, 180401 (2013).
[38] L. M. K. Vandersypen and I. L. Chuang, Rev. Mod. Phys. **76**, 1037 (2005).
[39] S. Kotler, N. Akerman, Y. Glickman, A. Keselman, and R. Ozeri, Nature **473**, 61 (2011).